frontiers | Frontiers in Materials

TYPE Original Research
PUBLISHED 25 September 2023
DOI 10.3389/fmats.2023.1245685

OPEN ACCESS

EDITED BY
Lei Zhang,
Xi'an Jiaotong University, China

REVIEWED BY
Yongzhi Cheng,
Wuhan University of Science and Technology, China
Mohammad Alibakhshikenari,
Universidad Carlos III de Madrid de Madrid, Spain
Muhammad Abuzar Baqir,
COMSATS University Islamabad, Sahiwal campus, Pakistan

*CORRESPONDENCE
Ayman A. Althuwayb,
aaalthuwayb@ju.edu.sa
Yung-Cheol Byun,
ycb@jeju.ac.kr
Dag Øivind Madsen,
dag.oivind.madsen@usn.no

RECEIVED 23 June 2023
ACCEPTED 07 September 2023
PUBLISHED 25 September 2023

CITATION
Althuwayb AA, Rashid N, Elhamrawy OI, Kaaniche K, Khan I, Byun Y-C and Madsen DØ (2023), Design and performance evaluation of a novel metamaterial broadband THz filter for 6G applications.
Front. Mater. 10:1245685.
doi: 10.3389/fmats.2023.1245685

Design and performance evaluation of a novel metamaterial broadband THz filter for 6G applications

Ayman A. Althuwayb[1]*, Nasr Rashid[1], Osama I. Elhamrawy[1], Khaled Kaaniche[1], Imran Khan[2,3], Yung-Cheol Byun[4]* and Dag Øivind Madsen[5]*

[1]Department of Electrical Engineering, College of Engineering, Jouf University, Sakaka, Kingdom of Saudi Arabia, [2]Department of Electrical Engineering, University of Engineering and Technology Peshawar, Peshswar, Pakistan, [3]Islamic University Centre for Scientific Research, The Islamic University, Najaf, Iraq, [4]Department of Computer Engineering, Jeju National University, Jeju City, Republic of Korea, [5]University of South-Eastern Norway, Kongsberg, Norway

Terahertz (THz) radiation, which has applications in the imaging of objects, non-destructive testing, satellite communication, medical diagnostics, and biosensing, has generated a great deal of attention due to its remarkable properties. This paper proposes a novel broadband filter for THz applications. The main idea is to overcome the insertion loss and bandwidth issues by modeling a frequency-domain finite difference method and guided-mode resonance (GMR). The optimal design scheme of the wideband pass filter based on the circular resonant ring is discussed by comparing the transmission parameters under various parameters. This scheme overcomes the restriction of the narrow passband bandwidth of the prior THz filters and achieves approximately 3 dB bandwidth of 0.54 THz. The proposed THz filter paper also has the advantages of a straightforward structure, low processing costs, and ease of conformal with other structures, and it can be used for stealth fighters, new communication technology, and precise instruments. In addition, when compared to existing models, the suggested filter offers higher 3 dB BW operation, increased transmittance, low insertion loss, and stable performance at various oblique angles.

KEYWORDS

terahertz, metamaterial, electromagnetic spectrum, broadband filter, 6G communication, guided-mode resonance, band pass filter, surface plasmon

1 Introduction

Electromagnetic waves with frequencies ranging from 0.1 to 10 THz are referred to as terahertz waves, which are electromagnetic waves with wavelengths between millimeter waves and infrared light, also known as submillimeter waves (Zhu et al., 2020; Saraereh, 2021; Luo et al., 2022). Because the frequency of the submillimeter wave band is more than 103 times higher than that of the millimeter wave band (the band used for 5G communication), the resources are abundant and the system capacity is large, so 6G technology selects the frequency in this band to achieve faster communication (Alibakhshike et al., 2021; Alibakhshikenari et al., 2022a; Sun et al., 2023). It can be seen that terahertz technology will provide crucial technical support for the development of a new generation of communication technology (Alibakhshikenari et al., 2021a; Althuwayb et al., 2021).

Electromagnetic metamaterials, also known as new artificial electromagnetic media, metamaterials, *etc.* (Alibakhshikenari et al., 2019a; Alibakhshikenari et al., 2020a; Alibakhshikneari et al., 2020; Alibakhshikenari et al., 2020b; Alibakhshikenari et al., 2020c; Alibakhshikenari et al., 2021b), are characterized by arranging artificial unit structures (artificial atoms) with sub-wavelength scales in a periodic or non-periodic manner, and then obtaining materials beyond the limits of natural materials. Electromagnetic properties, such as negative refractive index, zero refractive index, ultra-high refractive index, high-frequency magnetic response, *etc.* (Baqir and Choudhury, 2017; Alibakhshikenari et al., 2019b; Alibakhshikenari et al., 2019c; Alibakhshikenari et al., 2019d; Alibakhshikenari et al., 2022b). The research on the basic theory, functional devices and engineering applications of electromagnetic metamaterials has aroused extensive research interests in the fields of physics, information and materials (Baqir, 2019; Baqir, 2020; Pan et al., 2022a; Baqir and Choudhury, 2022; Liu et al., 2023). Based on the designable electromagnetic parameters and distribution of metamaterials, researchers have developed various new devices such as metamaterial cloaks, lenses, and antennas (Li et al., 2021a; Wang et al., 2022a; Yang et al., 2022; Zhao and Wang, 2022; Wang et al., 2023a). According to the field localization and field enhancement characteristics of metamaterials (this effect is especially significant in surface plasmon metamaterials) and subwavelength scale characteristics (Li et al., 2020a; Wang et al., 2022b; Cao, 2022; Liu et al., 2022; Xie et al., 2023), a novel metamaterial sensing and imaging device has been developed, which can effectively improve the sensor's performance. Sensitivity and imaging resolution (Cheng et al., 2016a; Huang et al., 2020; Li et al., 2021b; Xu et al., 2021; Feng et al., 2022). With the proposal and realization of digital coding and programmable metamaterials, the characterization and design of metamaterials are carried out in binary digital mode (that is, digital 0 and 1), which promotes the integration of metamaterials and information technology, making the new system superhuman. Material imaging system and communication system become possible (Li et al., 2021c; Zhao et al., 2022; Jiang et al., 2023; Liu and Xu, 2023; Xu and Liu, 2023).

The terahertz frequency region is between microwave and far-infrared in the electromagnetic spectrum, and is usually defined as electromagnetic radiation of 0.1–10 THz (Cao et al., 2021; Li et al., 2021d; Pan et al., 2022b; Chung et al., 2022; Ding et al., 2023). With the rapid development of terahertz sources and detectors and the continuous development of terahertz functional devices, terahertz science and technology have achieved vigorous development in recent years. Terahertz technology has good application prospects in material characterization, security inspection, biomedical imaging and communication (Yao et al., 2023; Zhang et al., 2022a; Liu, 2023; Zang et al., 2021; Li et al., 2020b). Among them, in terms of imaging, compared with microwave and millimeter wave frequencies, terahertz imagers will have higher spatial resolution, and compared with optical imaging, terahertz radiation has better penetration, so it can obtain more depth information (Liu et al., 2013; Wang et al., 2022c; Wang et al., 2022d; Liao et al., 2022; Wang et al., 2023b). At the same time, because this is a kind of non-ionizing radiation, it has better biological safety, so the application of terahertz imaging has been widely concerned (Jiang and Li, 2022; Xu et al., 2023; Zhang et al., 2023; Zhou et al., 2023). Terahertz metamaterials and metasurfaces have broad application prospects in terahertz imaging systems due to their sub-wavelength unit scale and flexible manipulation of electromagnetic wave amplitude, phase and polarization characteristics (Cheng et al., 2016b; Hosseininejad et al., 2018; Wang et al., 2019; Li et al., 2021e; Shen et al., 2022; Xi et al., 2022; Li et al., 2023; Miaofen et al., 2023).

In fact, researchers conducted in-depth research on THz waves, and developed many THz devices, such as THz absorbers (Zhao et al., 2019a; Ulla et al., 2019; Fajr et al., 2020; Lee and Jeong, 2020), THz antennas (Geim and Novoselov, 2007; Diaz and Carrier, 2012), THz reflector (Carrier et al., 2013; Danciu et al., 2019; Zhang et al., 2021; Leitenstorfer et al., 2023), *etc.*, and various THz systems, such as THz security detector (Strinati et al., 2019; Zhang et al., 2019; Akhtar et al., 2020), ultra-wideband THZ transmitter (Yi et al., 2019; Chen et al., 2020a; Zou and Chen, 2020), terahertz imaging system (Ullah et al., 2019; Jiao et al., 2020; Huang et al., 2023), *etc.*, they can be applied is widely used in security inspection, communication (Jiang et al., 2017; Lu et al., 2020; Manjappa and Singh, 2020; Rizza and Molle, 2022; Wu and Lin, 2023), biomedicine (Zhang et al., 2022b) and many other fields. Filter, as one of the most widely used key devices in THz communication technology (Chen et al., 2020b), has attracted the close attention of many researchers. The authors in (Wang et al., 2018) used a waveguide bandpass filter made of a two-dimensional square metal photonic crystal plate structure to achieve filtering effects in the sub-terahertz band, and adjusted the parameters and lattice constants of the multilayer waveguide in the structure, making its 3 dB bandwidth reach about 0.0052 THz. However, the structure is too complicated, and there are many influencing parameters, so it is not easy to process and prepare. The authors in (Sun et al., 2020) designed a polarization-insensitive broadband terahertz bandpass filter using metamaterials with complementary resonant structures.

The filter can achieve the same filtering effect on terahertz waves under different incident polarization states, the maximum 3 dB bandwidth in the working frequency band can reach 0.405 THz, and the structure of the filter is simple and easy to prepare. However, its transmission coefficient in the working frequency band is low, resulting in high electromagnetic wave loss. Reference (Kumar et al., 2019) also developed a THz filter using a coupled complementary metamaterial structure, with a 3 dB bandwidth of 0.39 THz. The authors in (Fahad et al., 2019) used the Koch curve fractal structure filter model for simulation analysis, and obtained a THz filter with a center frequency of 0.715 THz and a 3 dB bandwidth of 0.021 THz, but the filter fractal structure of the Koch curve is too complex, and the 3 dB bandwidth is narrow (Zhao et al., 2019b; Jiang et al., 2020).

Although the research work on THz broadband filters has been widely reported so far, according to the above literature analysis, it can be found that the current THz broadband filters still have complex structures, narrow bandwidth, low transmittance, high loss, *etc.* In view of this, this paper proposes a novel filter design with significant features. The main contributions are as follows.

- Design a new bimetallic ring electromagnetic metamaterial terahertz broadband bandpass filter based on guided-mode resonance (GMR);

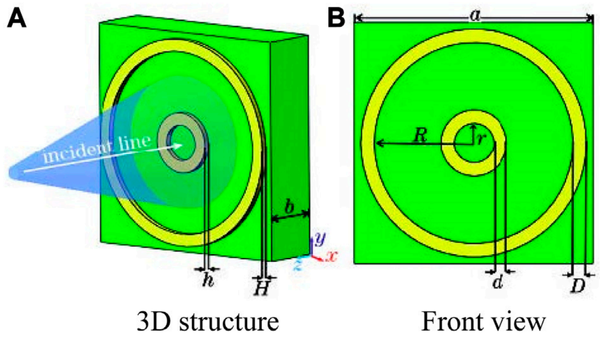

FIGURE 1
Proposed THz filter design. **(A)** 3D structure, **(B)** Front view.

- Optimize the electromagnetic response of the filter structure parameters to THz waves through simulation, so that it has both broadband and high transmittance characteristics;
- The structure of the filter is simple and easy to process, which provides a novel design scheme for THz filtering technology.

2 Filter design

The resonant unit of the THz filter designed in this paper is composed of a two-layer structure, as shown in Figure 1. The substrate material is a flexible polyimide film, and its dielectric constant ε and magnetic permeability μ are 3.5 and 1, respectively. The substrate shape is a cuboid with period length *a* and thickness *b*. The upper surface of the substrate is inlaid with two rings of different sizes, wherein: the inner diameter of the small ring is *r*, the width of the ring is *d*, and the thickness of the ring is *h*. The inner diameter of the large ring is *R*, the width of the ring is *D*, and the thickness is *H*. The material of the ring material is copper whose conductivity of the is set to be 5.96×10^7 S/m, which is close to the measured value for copper with the surface height.

(a) 3D structure b) Front view

The design structure of the single-layer THz filter involved in this paper is a theoretical model of artificially synthesized metamaterials. The mechanism of this model structure to achieve filtering characteristics in a certain frequency band of the THz frequency is the surface of the model that constitutes the frequency selective surface (FSS), and it has a frequency-selective effect on the incident electromagnetic wave. In this paper, the frequency domain finite difference (FDFD) software is used to carry out simulation experiments. The THz wave is vertically incident on the filter surface and the metamaterial structure has different electromagnetic response characteristics at different frequency points. The transmission coefficient decreases rapidly at the resonant frequency point, and will maintain a large value at other non-resonant frequency points, resulting in a very obvious trough in the transmission coefficient near the resonant frequency point. At the resonant frequency point, terahertz waves can hardly pass through, but at the non-resonant frequency point, a large number of THz waves can be perfectly transmitted. The above is the principle that the metamaterial structure can form a bandpass filter. Generally speaking, once the parameters of a terahertz filter made of metamaterials are determined, the filter can only work within a certain fixed frequency. By simulating the parameters of the filter and combining them with each other, the wideband pass filter with the best performance can be obtained.

3 Performance evaluation

3.1 Influence of inner ring radius *r*

Firstly, the effect of the radius *r* of the inner ring of the filter structure on its filtering performance is studied. The radius *r* of the inner ring is chosen to be 10, 20, 30, 40, 50 μm, respectively. The remaining structural parameters are set as follows: period length a = 180 μm, substrate height b = 50 μm, outer ring radius R = 80 μm, outer ring width D = 5 μm, outer ring thickness H = 4 μm, inner ring width d = 5 μm, inner ring thickness h = 4 μm. On the lateral sides of the unit, periodic boundary conditions are specified in order to produce an infinite metasurface. The open boundary is defined in the meantime to get rid of the reflection from the front and back faces. A periodic structure in the unbounded x-y plane is illuminated by an unlimited plane wave in the simulation, which is based on Floquet's principle. If the dimension of the device does not match the spot size of the incident wave, as it does in our simulations, scattering must be taken into account for a filter with a finite number of periodic units.

In the frequency range of 0~1.2 THz, the performance of the filter is simulated and calculated when the radius *r* of the inner ring of the resonant ring of the structure is changed, and the simulation results (S_{21} parameters) of the filter are obtained, as shown in Figure 2. Figure 2A reflects the transmission coefficient, and Figure 2B reflects the insertion loss. It can be seen that within the frequency range of 0–1.2 THz, the working center frequency of the filter moves to the low frequency direction with the increase of the inner ring radius *r*. When the inner ring radius *r* is in the range of 10–30 μm, the 3 dB bandwidth is larger, and the THz wave filter also has a higher transmission coefficient in its working frequency band. When the inner ring radius r = 20 μm, the 3 dB bandwidth reaches the maximum value, and the filter can obtain a larger working bandwidth. After comparing the simulation results, this paper selects the inner ring radius *r* as 20 μm.

3.2 Effect of outer ring radius *R*

Through the simulation of the above structural parameters, it is found that adjusting the parameters of the ring-shaped resonant structure on the surface of the filter can effectively change its filtering performance. Therefore, when the radius *r* of the inner ring is set to 20 μm and other structural parameters remain unchanged, the value of the radius *R* of the outer ring (40, 50, 60, 70, 80 μm, respectively) is changed for simulation. The simulation result is shown in Figure 3.

It can be seen from Figure 3 that as the outer ring radius *R* gradually increases, the filter center frequency f_0 moves from the

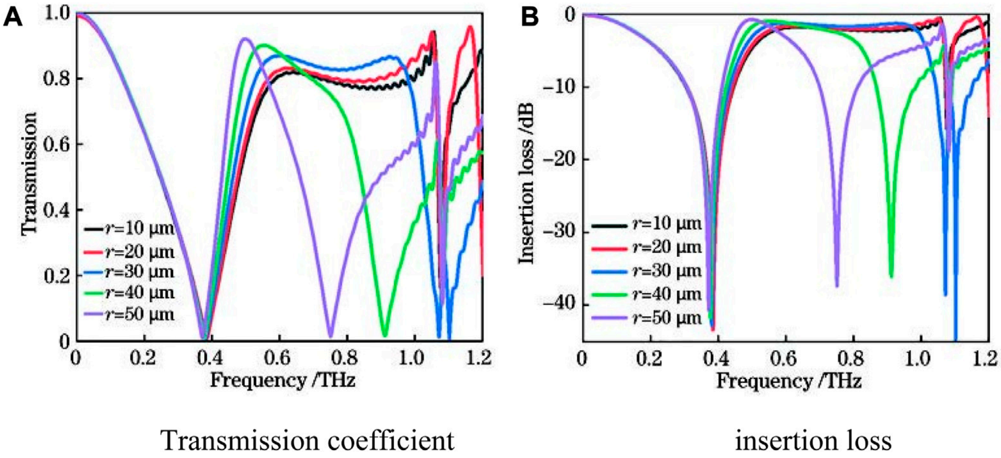

FIGURE 2
Impact of r on **(A)** transmission coefficient and **(B)** insertion loss.

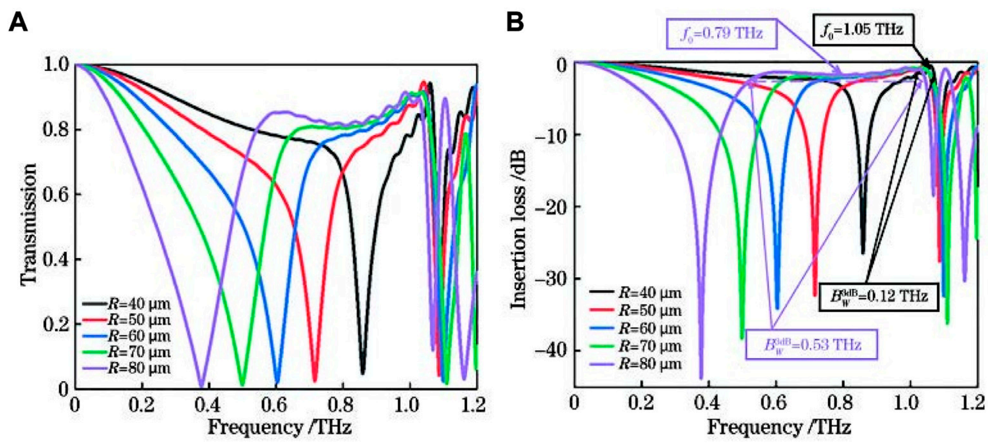

FIGURE 3
Impact of R on **(A)** transmission coefficient and **(B)** insertion loss.

high frequency direction to the low frequency direction, and its 3 dB bandwidth (B3dBW) increases greatly, from 0.12 THz to 0.53 THz. This shows that, while keeping other structural parameters unchanged, increasing the outer ring radius R can significantly improve the passband performance of the terahertz filter. However, the size of the outer ring radius R needs to match the structural parameters of the overall filter, and continuously increasing the outer ring radius will lead to the destruction of the overall performance of the filter. After comparative analysis, this paper chooses R = 80 μm as the optimal structural parameter.

3.3 Effect of outer ring width *D*

In order to analyze the role of the surface ring resonant structure in the overall structure of the terahertz filter in detail, this paper further discusses the influence of the width of the outermost ring structure on the overall performance of the filter. Under the condition that the radius of the outer ring is R = 80 μm and other structural parameters remain unchanged, the width D of the outer ring is selected to be 0, 10, 20, 30, and 40 μm for simulation, and the results shown in Figure 4 are obtained. The results show the transmission parameters of the metamaterial unit for different outer ring width D. It can be seen that the center frequency f_0 of the terahertz filter shifts from 0.715 THz to 1.1 THz with the increase of the outer ring width D, the center frequency increases gradually, and the 3 dB bandwidth increases with the increase of the outer ring width D decrease. When D is 0 μm, the transmission coefficient of the terahertz filter is the largest, and the 3 dB bandwidth also reaches the maximum. When D is 0 μm, the best filtering effect under ideal conditions can be achieved, but considering the technological conditions of post-processing, this paper takes D as a small value as much as possible, here D is 5 μm.

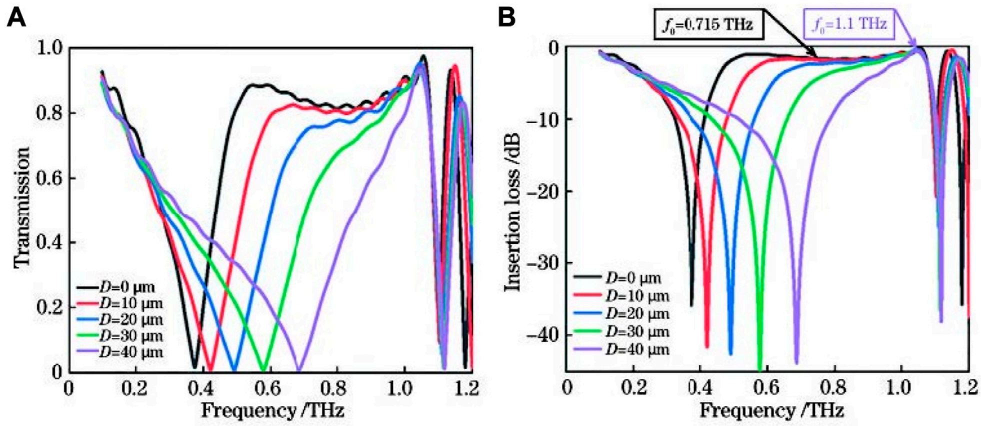

FIGURE 4
Impact of *D* on **(A)** transmission coefficient and **(B)** insertion loss.

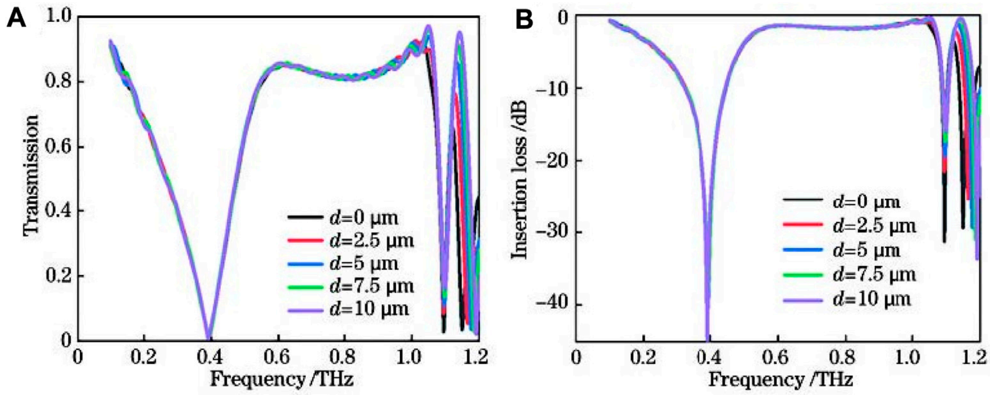

FIGURE 5
Impact of *d* on **(A)** transmission coefficient and **(B)** insertion loss.

3.4 Effect of inner ring width *d*

The small ring also plays an important role in the overall filtering effect of the filter for the resonant structure, so this paper simulates and optimizes the width of the inner ring. Set the rest of the structural parameters unchanged, the width d of the inner ring is 0, 2.5, 5, 7.5, and 10 μm, respectively, and the corresponding transmission coefficient of the terahertz filter is shown in Figure 5.

It can be seen from Figure 5 that as the inner ring width increases from 0 μm to 10 μm, the transmission effect of terahertz waves is almost the same. It can be seen that the change of the inner ring width in the range of 0–10 μm has little effect on the performance of the whole filter. In order to reduce the processing difficulty of the THz filter, the same structural parameters as the outer ring width *D* can be selected, that is, $d = D = 5$ μm.

3.5 Effect of period length *a*

This subsection will analyze the effect of the period length *a* of the structural unit of the THz filter on the overall performance of the filter. In the case of keeping the above ring resonance structure and other structural parameters unchanged, change the period length of the THz filter structural unit (choose a to be 180, 200, 220, 240, 260 μm respectively), and the obtained results are shown in Figure 6.

It can be seen from Figure 6 that the increase of the period length of the structural unit has no obvious effect on the low-order resonance of the filter at low frequencies, but it will change its high-order resonance at high frequencies, and the high-order resonance frequency increases with the period length increase in λ moves from 1.18 THz to 0.82 THz, resulting in a decrease in the 3 dB bandwidth width. To ensure that the filter has a high 3 dB bandwidth, this paper selects the period length *a* of the structural unit as 180 μm, so that it has better filtering performance.

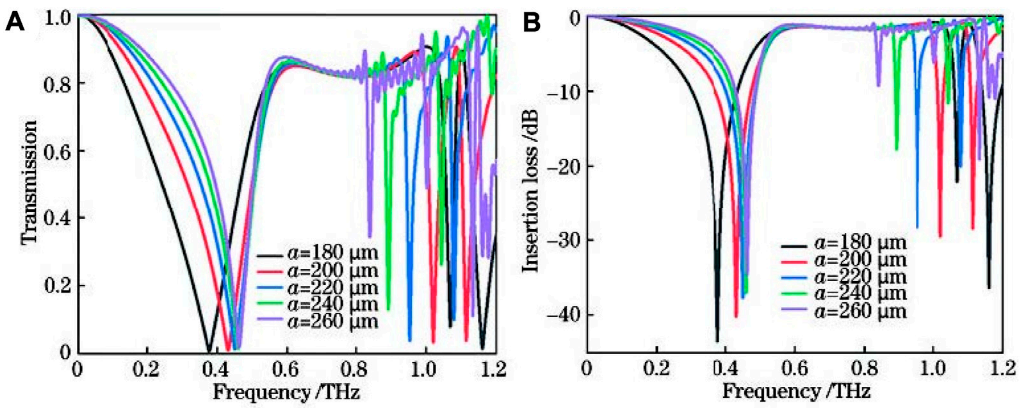

FIGURE 6
Impact of *a* on **(A)** transmission coefficient and **(B)** insertion loss.

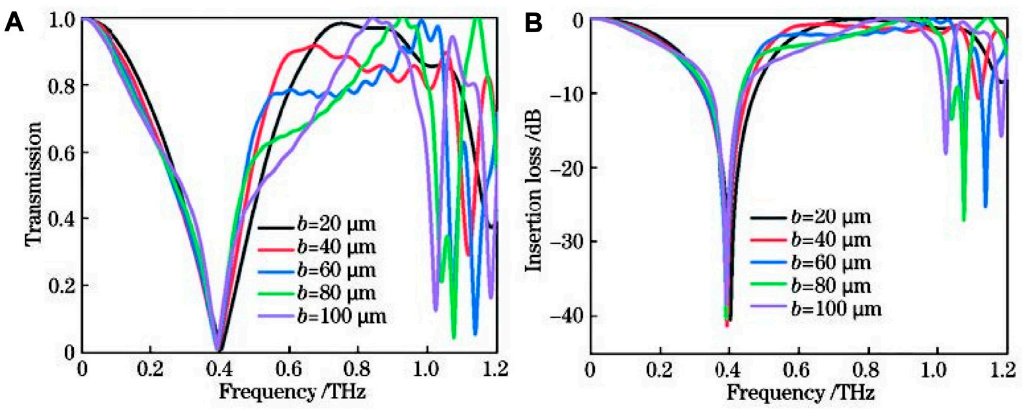

FIGURE 7
Impact of *b* on **(A)** transmission coefficient and **(B)** insertion loss.

3.6 Influence of substrate thickness *b*

The substrate of the THz filter is polyimide flexible material, and its thickness will directly affect whether the device can easily conform to other structures when it is used later. Therefore, under the condition that the above structural parameters remain unchanged, this paper conducts simulations while changing the substrate thickness b (i.e., b is 20, 40, 60, 80, 100 μm, respectively). Figure 7 shows the transmission parameters of metamaterial elements with varying substrate thickness b. It can be seen from Figure 7 that when the substrate thickness is 20–40 μm, the filter has better filtering performance. As the substrate thickness continues to increase, the ripple fluctuation in the filter band becomes more obvious, and the 3 dB bandwidth width also increases. For continuously increasing the filter substrate thickness does not improve its filtering performance. Therefore, the thickness of the substrate selected in this paper is 40 μm, which can obtain a more flexible overall structure while ensuring that the filter has better filtering performance and stable mechanical structure. It can be perfectly attached to satellites, spacecraft, wireless surface of complex structures such as human and machine, thus broadening its practical application value. The insertion loss also has better performance when b = 40 μm and its performance gets degraded for

TABLE 1 Specific parameters of the THz filter.

Parameter	Value (μm)
R	80
D	5
r	20
d	5
h/H	4
Length of substrate a	180
Thickness of substrate b	40

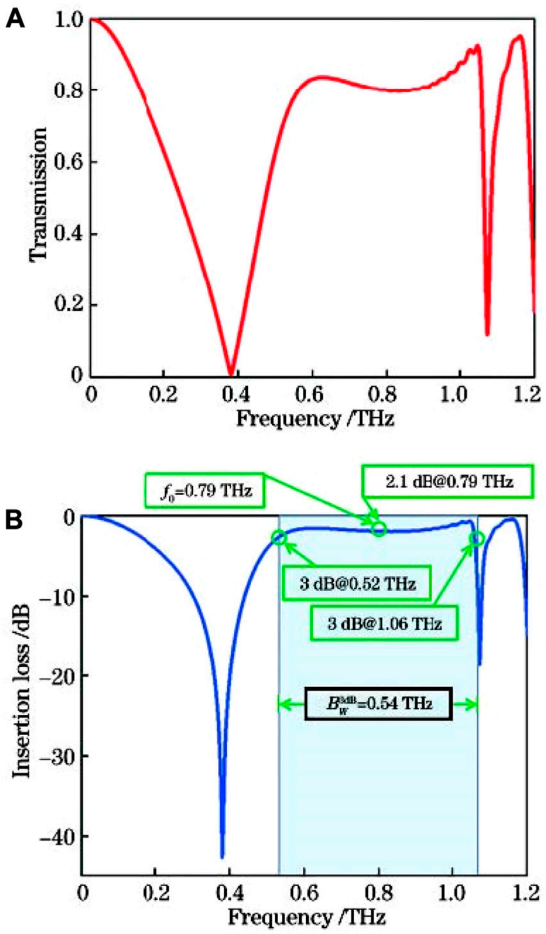

FIGURE 8
Impact of center frequency on **(A)** transmission coefficient and **(B)** insertion loss.

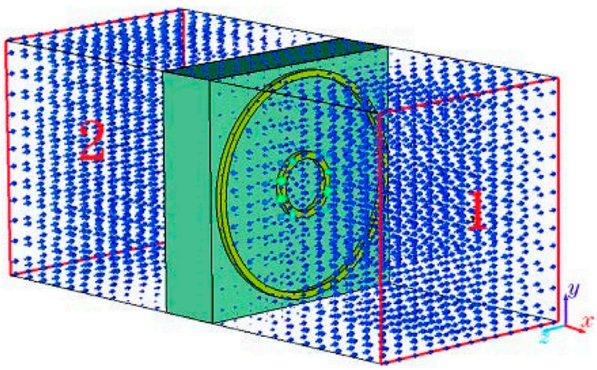

FIGURE 9
Illustration of E-field distribution.

higher thickness values. Therefore, we conclude that to get optimal filtering performance from this structure, the thickness should be 40 μm.

3.7 Analysis of the overall structure parameters

In summary, the specific parameters of the terahertz filter are obtained, as shown in Table 1. The frequency domain finite difference simulation software is used for simulation, and the transmission coefficient and insertion loss of the terahertz filter are obtained, as shown in Figure 8.

It can be seen from Figure 8 that the center frequency of the filter is 0.79 THz, the passband is 0.52~1.06 THz, the 3 dB bandwidth is 0.54 THz, and the relative bandwidth reaches 68.3%. The insertion loss is less than 2.1 dB. Figure 9, Figure 10 are the simulated electric field distribution diagrams of the THz filter at the center frequency of 0.79 THz and the surface current distribution diagrams at 0.37, 0.79, and 1.06 THz, respectively. By analyzing the electric field distribution diagram of the filter near the center frequency, it can be found that when the THz wave reaches port 2 (negative direction of x-axis) from port 1 (positive direction of x-axis), the electric field distribution on the front and rear sides of the filter is roughly the same. Compared with the front side, the electric field intensity at the rear side of the filter has no obvious attenuation, which indicates that the filter has good passband characteristics at this time, and the THz wave realizes low-loss transmission in the passband.

In order to better understand the working mechanism of the terahertz filter, this paper selects the low-order resonance frequency (f = 0.37 THz), the center frequency (f = 0.79 THz) and the high-order resonance frequency of the THz filter respectively (see Figure 9). The surface current distribution at the frequency (f = 1.06 THz) was analyzed. By observing the surface current distribution at f = 0.37 THz, it can be found that: at the outer ring, the current starts from the left side of the central axis of the outer ring and divides into upper and lower parts, and flows through the upper half ring and the lower half ring at the same time to the outer ring. The right side of the central axis of the ring, and when the current passes near the vertices of the upper and lower half rings, the current intensity continues to increase. At the inner ring, the current starts from the right side of the central axis of the inner ring, flows through the upper and lower parts of the inner ring at the same time, and reaches the left side of the central axis of the inner ring, and its current distribution law is just opposite to that of the outer ring. It is precisely because the inner ring and the outer ring have opposite current flow directions, two sets of strong LC (inductance-capacitance) resonances are generated above and below the central axis of the filter surface, resulting in a low frequency of the filter at 0.37 THz order resonance. Similarly, at f = 1.06 THz, the surface of the filter has the same current distribution as that at the low-order resonance (f = 0.37 THz), but its current intensity is significantly weaker than that at the low-order resonance, less attenuation of the transmission spectrum leading to higher order resonances. Continuing to analyze the surface current distribution of the filter at the center frequency (f = 0.79 THz), it can be found that although the overall distribution of the surface current is not significantly different from the low-order resonance and the current distribution at the high-order resonance at this time, the current intensity is obviously weaker than the f current intensity at the first two frequencies, so that the filter has a lower resonance intensity in the working frequency band and can obtain higher passband characteristics.

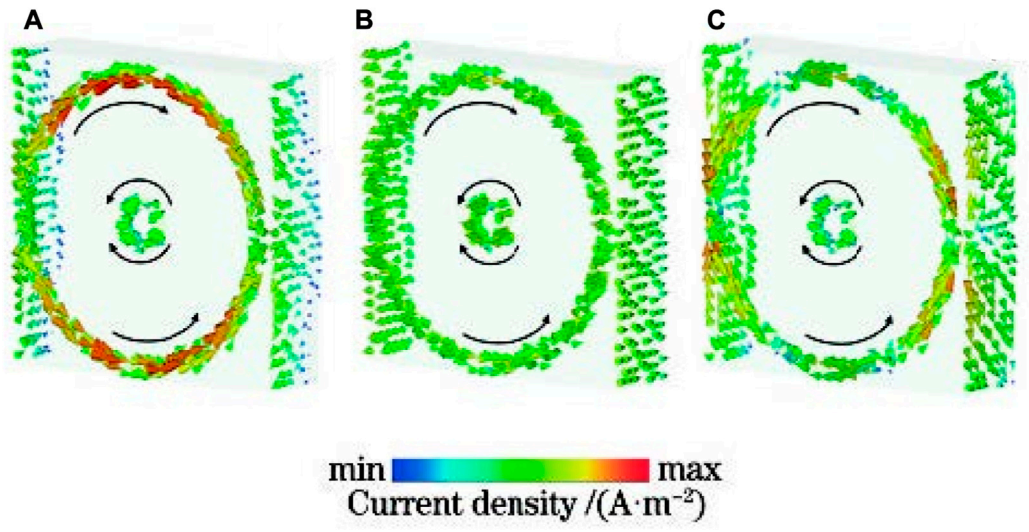

FIGURE 10
Comparison of surface current distribution. **(A)** 0.37 THz; **(B)** 0.79 THz; **(C)** 1.06 THz.

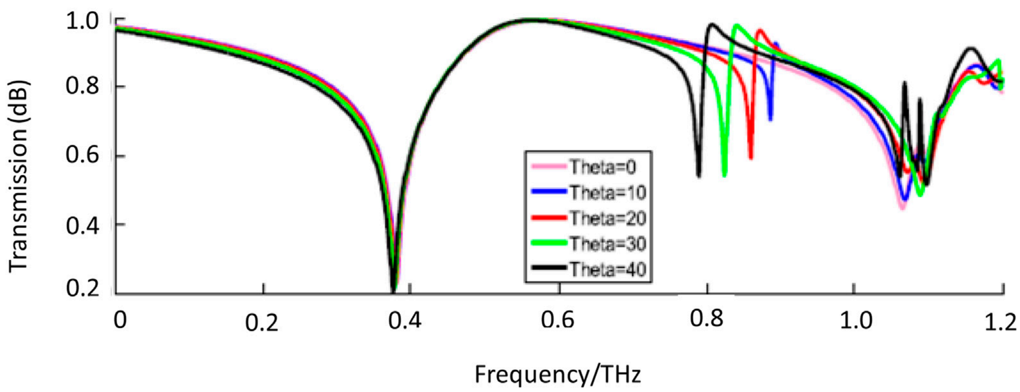

FIGURE 11
Transmission performance evaluation under different values incident angles.

Further analysis shows that the double-ring resonance structure can generate a low-order resonance and a high-order resonance in the range of 0–1.2 THz, the two resonance frequencies are far apart, and a transmission spectrum with a high degree of attenuation can be obtained at the resonance frequency. Therefore, the filter can obtain a wider operating bandwidth and better out-of-band rejection. At the same time, in the working frequency band of the filter, the resonance response of the structure is small, which ensures that the filter has a high transmission spectrum in the passband.

Figure 11 compared the transmission characteristics of the proposed filter structure under different incident angles. As can be seen from Figure 11, the transmission performance has stable performance for different incident angles which indicates its effectiveness.

Table 2 shows the comparison between the results of terahertz filters in recent years and the results of this paper.

4 Conclusion

In this paper, a metamaterial THz filter with a double ring structure is designed, and then the parameters of the filter are simulated and tested using electromagnetic simulation software. The transmission parameters are analyzed, and the parameters of the resonant ring and the substrate effect of each parameter on the performance of the terahertz filter are evaluated. By comparing the transmission parameters under various parameters, the optimal design scheme of the wideband pass filter based on the circular resonant ring is discussed, which breaks through the limitation of the narrow passband bandwidth of the previous THz filters, and obtains about 3 dB bandwidth of 0.54 THz. In addition, the proposed THz filter paper has the characteristics of simple structure, low processing cost, easy conformal with other structures, and can be applied to stealth fighters, new communication equipment and precision instruments. Furthermore, the proposed filter has the advantages of higher 3 dB BW

TABLE 2 Performance comparison of proposed and existing designs.

Ref	Operating frequency (THz)	3 dB BW (THz)	Central frequency (THz)	Transmittance (%)	Insertion loss (dB)	Applications	Complexity
Wang et al. (2018)	0.1 to 0.16	0.0052	0.145	-	≤ 0.95	Hollow pipe THz transmission	High
						Waveguides	
Sun et al. (2020)	0.1 to 0.6	0.16	0.42	≤ 78	-	THz sensors	High
Kumar et al. (2019)	0.2 to 2	0.39	0.69	≤ 98	-	THz spectroscopy	Medium
Fahad et al. (2019)	-	0.021	0.715	≤ 92	-	Biosensors and communication systems	High
Zhao et al. (2019b)	0.2 to 1.8	0.15	0.66	≤ 84.4	-	THz imaging, sensing, and astronomy exploration	Medium
	0.3 to 1.1	0.29	0.56	≤ 81.7			
Proposed	0 to 1.2	0.54	0.79	≤ 93	≤ 2.1	6G application, satellites, spacecraft, wireless surface of complex structures such as HMI	Low

operation, improved transmittance, low insertion loss and stable performance under different oblique angles as compared with existing models. In the follow-up research, we will consider other parameters to evaluate the performance of the filter.

Data availability statement

The original contributions presented in the study are included in the article/supplementary material, further inquiries can be directed to the corresponding authors.

Author contributions

Conceptualization: AA Data Curation: NR Methodology: OE Writing original draft: KK Project administration: IK Supervision and funding acquisition: DM. All authors contributed to the article and approved the submitted version.

Funding

This research was financially supported by the Ministry of Small and Medium-sized Enterprises (SMEs) and Startups (MSS), Korea, under the "Regional Specialized Industry Development Plus Program (R&D, S3246057)" supervised by the Korea Technology and Information Promotion Agency for SMEs (TIPA). This work was also financially supported by the Ministry of Trade, Industry and ENERGY (MOTIE) through the fostering project of The Establishment Project of Industry-University Fusion District.

Conflict of interest

The authors declare that the research was conducted in the absence of any commercial or financial relationships that could be construed as a potential conflict of interest.

Publisher's note

References

Akhtar, M., Hassan, S., Ghaffar, R., Jung, H., Garg, S., and Hossain, M. S. (2020). The shift to 6G communications: vision and requirements. *Human-centric Comput. Inf. Sci.* 10 (53), 53–27. doi:10.1186/s13673-020-00258-2

Alibakhshikenari, M., Virdee, B., Althuwayb, A., Mariyanayagam, D., and Limiti, E. (2021). Compact and low-profile on-chip antenna using underside electromagnetic coupling mechanism for terahertz front-end transceivers. *Electronics* 10 (11), 1264–1318. doi:10.3390/electronics10111264

Alibakhshikenari, M., Ali, E., Soruri, M., Dalarsson, M., Naser-Moghadasi, M., Virdee, B. S., et al. (2022a). A comprehensive survey on antennas on-chip based on metamaterial, metasurface, and substrate integrated waveguide principles for millimeter-waves and terahertz integrated circuits and systems. *IEEE Access* 10, 3668–3692. doi:10.1109/access.2021.3140156

Alibakhshikenari, M., Parchin, N., Virdee, B., See, C., et al. (2020c). High performance metasurface-based on-chip antenna for terahertz integrated circuits, third international workshop on mobile terahertz systems (IWMTS). *Essen* 1–2. doi:10.1109/IWMTS49292.2020.9166324

Alibakhshikenari, M., Virdee, B., Alhameed, R., Falcon, F., et al. (2022b). Overcome the limitations of performance parameters of on-chip antennas based on metasurface and coupled feeding approaches for applications in system-on-chip for THz integrated-circuits. *IEEE Asia-Pacific Microw. Conf. (APMC)*. doi:10.1109/APMC46564.2019.9038524

Alibakhshikenari, M., Virdee, B., Althuwayb, A., Aissa, S., See, C., Abd-Alhameed, R. A., et al. (2021b). Study on on-chip antenna design based on metamaterial-inspired and substrate-integrated waveguide properties for millimetre-wave and THz integrated-circuit applications. *J. Infrated, Millim. Terahertz Waves* 42, 17–28. doi:10.1007/s10762-020-00753-8

Alibakhshikenari, M., Virdee, B., Salekzamankhani, S., Aissa, S., See, C., Soin, N., et al. (2021a). High-isolation antenna array using SIW and realized with a graphene layer for sub-terahertz wireless applications. *Sci. Rep.* 11 (10218), 10218–10317. doi:10.1038/s41598-021-87712-y

Alibakhshikenari, M., Virdee, B., See, C., Alhameed, R., et al. (2019a). *A novel 0.3-0.31 THz GaAs-based transceiver with on-chip slotted metamaterial antenna based on SIW technology*. Singapore: IEEE Asia-Pacific Microwave Conference, 69–71.

Alibakhshikenari, M., Virdee, B., See, C., Alhameed, R., Falcon, F., et al. (2019b). High-performance 50 μm silicon-based on-chip antenna with high port-to-port isolation implemented by metamaterial and SIW concepts for THz integrated systems. *Int. Congr. Artif. Mater. Nov. Wave Phenom. – Metamaterials* 16, 23–25. doi:10.1109/APMC46564.2019.9038524

Alibakhshikenari, M., Virdee, B., See, C., Alhameed, R., Falcon, F., et al. (2019c). Silicon-based 0.450-0.475 THz series-fed double dielectric resonator on-chip antenna array based on metamaterial properties for integrated-circuits. *Int. Congr. Artif. Mater. Nov. Wave Phenom. – Metamaterials* 16, 26–28. doi:10.1109/MetaMaterials.2019.8900949

Alibakhshikenari, M., Virdee, B., See, C., Alhameed, R., and Limiti, E., "High performance on-chip array antenna based on metasurface feeding structure for terahertz integrated circuits," 44th International Conference on Infrared, Millimeter, and Terahertz Waves (IRMMW-THz), Paris, France, 1-6 September, IEEE, pp. 11–17. 2019d.

Alibakhshikenari, M., Virdee, B., See, C., Alhameed, R., Falcone, F., and Limiti, E. (2020b). High-gain metasurface in polyimide on-chip antenna based on CRLH-TL for sub-terahertz integrated circuits. *Sci. Rep.* 10 (4298), 4298–4316. doi:10.1038/s41598-020-61099-8

Alibakhshikenari, M., Virdee, B., See, C., Shukla, P., Salekzamankhani, S., Abd-Alhameed, R. A., et al. (2020a). Study on improvement of the performance parameters of a novel 0.41-0.47 THz on-chip antenna based on metasurface concept realized on 50 μm GaAs-layer. *Sci. Rep.* 10 (11034), 11034–11116. doi:10.1038/s41598-020-68105-z

Alibakhshikneari, M., Virdee, B., Khalily, M., See, C., Abd-Alhameed, R., Falcone, F., et al. (2020). High-gain on-chip antenna design on silicon layer with aperture excitation for terahertz applications. *IEEE Antennas Wirel. Propag. Lett.* 19 (9), 1576–1580. doi:10.1109/lawp.2020.3010865

Althuwayb, A., Alibakhshikenari, M., Virdee, B., Benetatos, H., Falcone, F., and Limiti, E. (2021). Antennas on chip (AoC) design using metasurface and SIW technologies for THz wireless applications. *Electronics* 10 (9), 1–18. doi:10.3390/electronics10091120

Baqir, M., and Choudhury, P. (2022). Hyperbolic metamaterial-based optical biosensor for detecting cancer cells. *IEEE Photonics Technol. Lett.* 35 (4), 183–186. doi:10.1109/lpt.2022.3228943

Baqir, M., and Choudhury, P. (2017). Hyperbolic metamaterial-based UV absorber. *IEEE Photonics Technol. Lett.* 29 (18), 1548–1551. doi:10.1109/lpt.2017.2735453

Baqir, M. (2020). Conductive metal-oxide-based tunable, wideband, and wide-angle metamaterial absorbers operating in the near-infrared and short-wavelength infrared regions. *Appl. Opt.* 59 (34), 10912–10919. doi:10.1364/ao.411268

Baqir, M. (2019). Wide-band and wide-angle, visible-and near-infrared metamaterial-based absorber made of nanoholed tungsten thin film. *Opt. Mater. Express* 9 (5), 2358–2367. doi:10.1364/ome.9.002358

Cao, H. (2022). Entrepreneurship education-infiltrated computer-aided instruction system for college music majors using convolutional neural network. *Front. Psychol.* 13, 900195. doi:10.3389/fpsyg.2022.900195

Cao, K., Wang, B., Ding, H., Lv, L., Dong, R., Cheng, T., et al. (2021). Improving physical layer security of uplink NOMA via energy harvesting jammers. *IEEE Trans. Inf. Forensics Secur.* 16, 786–799. doi:10.1109/TIFS.2020.3023277

Carrier, J. P., Tamagone, M., Diaz, J. G., and Carrasco, E. (2013). *Graphene antenna: Can integration and reconfigurability compensate for the loss?* Nuremberg, Germany: European Microwave Conference, 141–148.

Chen, X., Tian, Z., Lu, Y., Xu, Y., Zhang, X., Ouyang, C., et al. (2020a). Electrically tunable perfect terahertz absorber based on a graphene Salisbury screen hybrid metasurface. *Adv. Opt. Mater.* 8 (3), 1900660–1901771. doi:10.1002/adom.201900660

Chen, Y., Cheng, J., and Liang, C. (2020b). Switchable terahertz band-pass/band-stop filter enabled by hybrid vanadium dioxide metamaterial. *Adv. Condens. Matter Phys.* 20, 1–6. doi:10.1155/2020/3902835

Cheng, B., Zhu, D., Zhao, S., and Chen, J. (2016a). Situation-aware IoT service coordination using the event-driven SOA paradigm. *IEEE Trans. Netw. Serv. Manag.* 13 (2), 349–361. doi:10.1109/tnsm.2016.2541171

Cheng, B., Zhu, D., Zhao, S., and Chen, J. (2016b). Situation-Aware IoT service coordination using the event-driven SOA paradigm. *IEEE Trans. Netw. Serv. Manag.* 13 (2), 349–361. doi:10.1109/TNSM.2016.2541171

Chung, K. L., Tian, H., Wang, S., Feng, B., and Lai, G. (2022). Miniaturization of microwave planar circuits using composite microstrip/coplanar-waveguide transmission lines. *Alexandria Eng. J.* 61 (11), 8933–8942. doi:10.1016/j.aej.2022.02.027

Danciu, M., Stratulat, T., Stefanescu, C., Dodi, G., Tamba, B., et al. (2019). Terahertz spectroscopy and imaging: A cutting-edge method for diagnosing digestive cancers. *Materials* 12 (9), 1–24. doi:10.3390/ma12091519

Diaz, J., and Carrier, J. P. (2012).Microwave to THz properties of graphene and potential antenna applications IEEE International Symposium on Antennas and Propagation (ISAP), 2nd November 2023, Nagoya, Japan. IEEE, 239–242.

Ding, G., Anselmi, N., Xu, W., Li, P., Rocca, P., Zhang, S., et al. (2023). A pan-cancer analysis of the role of *WDFY2* in human tumors. *IEEE Antennas Wirel. Propag. Lett.*, 1–16. doi:10.1080/02648725.2023.2194077

Fahad, A., Ruan, C., and Cheng, K. (2019). A wideband terahertz transmissive polarization manipulator based on metasurfaces. *Electronics* 8 (10), 1–18. doi:10.3390/electronics8101068

Fajr, S., Rajawat, A., and Gupta, S. H. (2020). Design and optimization of THz antenna for onboardy wan applications. *Optik* 223, 165563–165612. doi:10.1016/j.ijleo.2020.165563

Feng, Y., Zhang, B., Liu, Y., Niu, Z., Fan, Y., and Chen, X. (2022). A D-band manifold triplexer with high isolation utilizing novel waveguide dual-mode filters. *IEEE Trans. Terahertz Sci. Technol.* 12 (6), 678–681. doi:10.1109/TTHZ.2022.3203308

Geim, A. K., and Novoselov, K. S. (2007). The rise of graphene. *Nat. Mater.* 6 (3), 183–191. doi:10.1038/nmat1849

Hosseininejad, S. E., Neshat, M., Dana, R., Lemme, M., Bolivar, P. H., et al. (2018). Reconfigurable THz plasmonic antenna based on few-layer graphene with high radiation efficiency. *Nanomaterials* 8 (8), 1–18. doi:10.3390/nano8080577

Huang, X., Zhou, L., Yuan, Y., Qiu, L., and Mao, J. (2020). Quintuple-mode W-band packaged filter based on a modified quarter-mode substrate-integrated waveguide cavity. *IEEE Trans. Components, Packag. Manuf. Technol.* 9 (11), 2237–2247. doi:10.1109/TCPMT.2019.2925371

Huang, Y., Shen, Y., and Wang, J. (2023). From terahertz imaging to terahertz wireless communications. *Engineering* 22 (3), 106–124. doi:10.1016/j.eng.2022.06.023

Jiang, M., Hu, F., Qian, Y., Zhang, L., Zhang, W., and Han, J. (2020). Tunable terahertz band-pass filter based on MEMS reconfigurable metamaterials. *J. Phys. D* 53 (6), 065107–065118. doi:10.1088/1361-6463/ab5751

Jiang, W., Wang, H., Xie, W., and Qu, Z. (2023). Lithography alignment techniques based on moiré fringe. *Photonics* 10, 351. doi:10.3390/photonics10040351

Jiang, Y., Deng, B., Qin, Y., Wang, H., and Liu, K. (2017). A fast terahertz imaging method using sparse rotating array. *Sensors* 17 (10), 2209–2218. doi:10.3390/s17102209

Jiang, Y., and Li, X. (2022). Broadband cancellation method in an adaptive co-site interference cancellation system. *Int. J. Electron.* 109 (5), 854–874. doi:10.1080/00207217.2021.1941295

Jiao, X., Zhang, Z., Li, T., Xu, Y., Song, G., and Sohn, E. H. (2020). Visualization of mouse choroidal and retinal vasculature using fluorescent tomato lectin perfusion. *Appl. Sci.* 10 (20), 1–18. doi:10.1167/tvst.9.1.1

Kumar, D., Kumar, R., and Chowdhury, D. (2019). Complementary metamaterials based broadband bandpass terahertz filter. *IEEE Int. Workshop Recent Adv. Photonics (WRAP)*, 13–14. doi:10.1016/j.rinp.2019.102887

Luo, Y., Yu, J., Cheng, Y., Chen, F., and Luo, H. (2022). A compact microwave bandpass filter on spoof surface plasmon polariton and substrate integrated plamonic waveguide structures. *Appl. Phys. A* 128 (97), 1159–1171. doi:10.1007/s00339-021-05250-w

Lee, C., and Jeong, J. (2020). THz cmos on-chip antenna array using defected ground structure. *Electronics* 9 (7), 1137–1214. doi:10.3390/electronics9071137

Leitenstorfer, A., Moskalenko, A., Kampfrath, T., Kono, J., Castro-Camus, E., Peng, K., et al. (2023). The 2023 terahertz science and technology roadmap. *J. Phys. D Appl. Phys.* 56 (22), 223001–223066. doi:10.1088/1361-6463/acbe4c

Li, A., Masouros, C., Swindlehurst, A. L., and Yu, W. (2021b). 1-Bit massive MIMO transmission: embracing interference with symbol-level precoding. *IEEE Commun. Mag.* 59 (5), 121–127. doi:10.1109/MCOM.001.2000601

Li, A., Masouros, C., Vucetic, B., Li, Y., and Swindlehurst, A. L. (2021c). Interference exploitation precoding for multi-level modulations: closed-form solutions. *IEEE Trans. Commun.* 69 (1), 291–308. doi:10.1109/TCOMM.2020.3031616

Li, B., Zhang, M., Rong, Y., and Han, Z. (2021d). Transceiver optimization for wireless powered time-division duplex MU-MIMO systems: non-robust and robust designs. *IEEE Trans. Wirel. Commun.* 21 (6), 4594–4607. doi:10.1109/TWC.2021.3131595

Li, C., Lin, L., Zhang, L., Xu, R., Chen, X., Ji, J., et al. (2021a). Long noncoding RNA p21 enhances autophagy to alleviate endothelial progenitor cells damage and promote endothelial repair in hypertension through SESN2/AMPK/TSC2 pathway. *Pharmacol. Res.* 173, 105920. doi:10.1016/j.phrs.2021.105920

Li, M., Wang, T., Chu, F., Han, Q., Qin, Z., and Zuo, M. J. (2021e). Scaling-basis chirplet transform. *IEEE Trans. Industrial Electron.* 68 (9), 8777–8788. doi:10.1109/TIE.2020.3013537

Li, Q., Lin, H., Tan, X., and Du, S. (2020b). H∞ consensus for multiagent-based supply chain systems under switching topology and uncertain demands. *IEEE Trans. Syst. Man, Cybern. Syst.* 50 (12), 4905–4918. doi:10.1109/TSMC.2018.2884510

Li, Q., Miao, Y., Zeng, X., Tarimo, C., Wu, C., and Wu, J. (2020a). Prevalence and factors for anxiety during the coronavirus disease 2019 (COVID-19) epidemic among the teachers in China. *J. Affect. Disord.* 277, 153–158. doi:10.1016/j.jad.2020.08.017

Li, Z., Kong, Y., and Jiang, C. (2023). A transfer double deep Q network based DDoS detection method for internet of vehicles. *IEEE Trans. Veh. Technol.* 72 (4), 5317–5331. doi:10.1109/TVT.2022.3233880

Liao, K., Lu, D., Wang, M., and Yang, J. (2022). A low-pass virtual filter for output power smoothing of wind energy conversion systems. *IEEE Trans. Industrial Electron.* 69 (12), 12874–12885. doi:10.1109/TIE.2021.3139177

Liu, A., Zhai, Y., Xu, N., Nie, W., Li, W., and Zhang, Y. (2022). Region-aware image captioning via interaction learning. *IEEE Trans. Circuits Syst. Video Technol.* 32 (6), 3685–3696. doi:10.1109/tcsvt.2021.3107035

Liu, B., Peng, Y., Jin, Z., Wu, X., Gu, H., Wei, D., et al. (2023). Terahertz ultrasensitive biosensor based on wide-area and intense light-matter interaction supported by QBIC. *Chem. Eng. J.* 462 (142347), 142347–142417. doi:10.1016/j.cej.2023.142347

Liu, D., Cao, Z., Jiang, H., Zhou, S., Xiao, Z., and Zeng, F. (2013). Concurrent low-power listening: A new design paradigm for duty-cycling communication. *ACM Trans. Sen. Netw.* 19 (1), 1–24. doi:10.1145/3517013

Liu, G. (2023). A Q-Learning-based distributed routing protocol for frequency-switchable magnetic induction-based wireless underground sensor networks. *Future Gener. Comput. Syst.* 139, 253–266. doi:10.1016/j.future.2022.10.004

Liu, Y., and Xu, K. (2023). Millimeter-wave bandpass filters using on-chip dual-mode resonators in 0.13 μm SiGe BiCMOS technology. *IEEE Trans. Microw. Theory Tech.* 71, 3650–3660. doi:10.1109/TMTT.2023.3242317

Lu, Y., Wang, X., Sun, W., Feng, S., Sheng, J., Han, P., et al. (2020). Reflective single-pixel terahertz imaging based on compressed sensing. *IEEE Trans. Terahertz Sci. Technol.* 10 (5), 495–501. doi:10.1109/tthz.2020.2982350

Manjappa, M., and Singh, R. (2020). Materials for terahertz optical science and technology. *Adv. Opt. Mater.* 8 (3), 1901984–1902593. doi:10.1002/adom.201901984

Miaofen, L., Youmin, L., Tianyang, W., Fulei, C., and Zhike, P. (2023). Adaptive synchronous demodulation transform with application to analyzing multicomponent signals for machinery fault diagnostics. *Mech. Syst. Signal Process.* 191, 110208. doi:10.1016/j.ymssp.2023.110208

Pan, S., Lin, M., Xu, M., Zhu, S., Bian, L., and Li, G. (2022a). A low-profile programmable beam scanning holographic array antenna without phase shifters. *IEEE Internet Things J.* 9 (11), 8838–8851. doi:10.1109/jiot.2021.3116158

Pan, S., Lin, M., Xu, M., Zhu, S., Bian, L., and Li, G. (2022b). A low-profile programmable beam scanning holographic array antenna without phase shifters. *IEEE Internet Things J.* 9 (11), 8838–8851. doi:10.1109/JIOT.2021.3116158

Rizza, C., and Molle, A. (2022). *Closing THz gap Dirac semimetals,"* Light Sci. Appl. 11 (124), 1–2. doi:10.1038/s41377-022-00812-w

Saraereh, O. A. (2021). A novel broadband antenna design for 5G applications. *Comput. Mater. Continua* 67 (1), 1121–1136. doi:10.32604/cmc.2021.015066

Shen, X., Jiang, H., Liu, D., Yang, K., Deng, F., Lui, J. C. S., et al. (2022). PupilRec: leveraging pupil morphology for recommending on smartphones. *IEEE Internet Things J.* 9 (17), 15538–15553. doi:10.1109/JIOT.2022.3181607

Strinati, E., Barbarossa, S., Gonzalez, J., Ktenas, D., Cassiau, N., Maret, L., et al. (2019). 6G: the next frontier: from holographic messaging to artificial intelligence using subterahertz and visible light communication. *IEEE Veh. Technol. Mag.* 14 (3), 42–50. doi:10.1109/mvt.2019.2921162

Sun, D., Qi, L., and Liu, Z. (2020). Terahertz broadband filter and electromagnetically induced transparency structure with complementary metasurface. *Results Phys.* 16 (2), 102887–103873. doi:10.1016/j.rinp.2019.102887

Sun, S., Cheng, Y., Luo, H., Chen, F., and Li, X. (2023). Notched-wideband bandpass filter based on spoof surface plasmon polaritons loaded with resonator structure. *Plasmonics* 18, 165–174. doi:10.1007/s11468-022-01755-z

Ullah, S., Ruan, C., Haq, T., and Zhang, X. (2019). High performance THz patch antenna using photonic band gap and defected ground structure. *J. Electromagn. Waves Appl.* 33 (15), 1943–1954. doi:10.1080/09205071.2019.1654929

Wang, B., Zhang, Y., and Zhang, W. (2022c). A composite adaptive fault-tolerant attitude control for a quadrotor UAV with multiple uncertainties. *J. Syst. Sci. Complex.* 35 (1), 81–104. doi:10.1007/s11424-022-1030-y

Wang, B., Zhu, D., Han, L., Gao, H., Gao, Z., and Zhang, Y. (2023b). Adaptive Fault-tolerant control of a hybrid canard rotor/wing UAV under transition flight subject to actuator faults and model uncertainties. *IEEE Trans. Aerosp. Electron. Syst.* 59, 4559–4574. doi:10.1109/TAES.2023.3243580

Wang, C., Yao, Y., Yu, J., and Chen, X. (2019). 3d beam reconfigurable THz antenna with graphene-based high impedance surface. *Electronics* 8 (11), 1291–1321. doi:10.3390/electronics8111291

Wang, F., Wang, H., Zhou, X., and Fu, R. (2022a). A driving fatigue feature detection method based on multifractal theory. *IEEE Sensors J.* 22 (19), 19046–19059. doi:10.1109/jsen.2022.3201015

Wang, H., Wang, K., Xue, Q., Peng, M., Yin, L., Gu, X., et al. (2022b). Transcranial alternating current stimulation for treating depression: A randomized controlled trial. *Brain* 145 (1), 83–91. doi:10.1093/brain/awab252

Wang, K., Zhang, B., Alenezi, F., and Li, S. (2022d). Communication-efficient surrogate quantile regression for non-randomly distributed system. *Inf. Sci.* 588, 425–441. doi:10.1016/j.ins.2021.12.078

Wang, N., Chang, T., Yang, Y., Zhang, J., Zhang, X., Gao, L., et al. (2018). Bending loss and propagation characterization of hollow pipe polymer terahertz waveguides. *Microw. Opt. Technol. Lett.* 60 (12), 2862–2869. doi:10.1002/mop.31440

Wang, Z., Ahmadi, A., Tian, H., Jafari, S., and Chen, G. (2023a). Lower-dimensional simple chaotic systems with spectacular features. *Chaos, Solit. Fractals* 169 (113299), 113299–114124. doi:10.1016/j.chaos.2023.113299

Wu, L., and Lin, Y. (2023). Flexible terahertz metamaterial filter with high transmission intensity and large tuning range for optical communication application. *Phys. E Low-dimensional Syst. Nanostructures* 146 (3), 115563–115578. doi:10.1016/j.physe.2022.115563

Xi, X., Xi, B., Miao, C., Yu, R., Xie, J., Xiang, R., et al. (2022). Factors influencing technological innovation efficiency in the Chinese video game industry: applying the meta-frontier approach. *Technol. Forecast. Soc. Change* 178, 121574. doi:10.1016/j.techfore.2022.121574

Xie, X., Tian, Y., and Wei, G. (2023). Deduction of sudden rainstorm scenarios: integrating decision makers emotions, dynamic bayesian network and DS evidence theory. *Nat. Hazards* 116, 2935–2955. doi:10.1007/s11069-022-05792-z

Xu, K., Guo, Y., Liu, Y., Deng, X., Chen, Q., and Ma, Z. (2021). 60-GHz compact dual-mode on-chip bandpass filter using GaAs technology. *IEEE Electron Device Lett.* 42 (8), 1120–1123. doi:10.1109/LED.2021.3091277

Xu, K., and Liu, Y. (2023). Millimeter-wave on-chip bandpass filter using complementary-broadside-coupled structure. *IEEE Trans. Circuits Syst. II Express Briefs* 70, 2829–2833. doi:10.1109/TCSII.2023.3255310

Xu, X., Sun, Y., Tian, X., Zhou, L., and Li, Y. (2023). A novel orientation determination approach of mobile robot using inertial and magnetic sensors. *IEEE Trans. Industrial Electron.* 70 (4), 4267–4277. doi:10.1109/TIE.2022.3177762

Yang, S., Li, Q., Li, W., Li, X., and Liu, A. (2022). Dual-level representation enhancement on characteristic and context for image-text retrieval. *IEEE Trans. Circuits Syst. Video Technol.* 32 (11), 8037–8050. doi:10.1109/tcsvt.2022.3182426

Yao, Y., Shu, F., Li, Z., Cheng, X., and Wu, L. (2023). Secure transmission scheme based on joint radar and communication in mobile vehicular networks. *IEEE Trans. Intelligent Transp. Syst.* 24, 10027–10037. doi:10.1109/TITS.2023.3271452

Yi, Z., Liang, C., Chen, X., Zhou, Z., Tang, Y., Ye, X., et al. (2019). Dual-band plasmonic perfect absorber based on graphene metamaterials for refractive index sensing application. *Micromachines* 10 (7), 443–518. doi:10.3390/mi10070443

Zhang, Y., He, Y., Wang, H., Sun, L., and Su, Y. (2021). Ultra-broadband mode size converter using on-chip metamaterial-based luneburg lens. *Metamaterial-Based Lunebg. Lens* 8 (1), 202–208. doi:10.1021/acsphotonics.0c01269

Zhang, C., Xiao, P., Zhao, Z., Liu, Z., Yu, J., Hu, X., et al. (2023). A wearable localized surface plasmons antenna sensor for communication and sweat sensing. *IEEE Sensors J.* 23 (11), 11591–11599. doi:10.1109/JSEN.2023.3266262

Zhang, J., Li, S., and Le, W. (2021). Advances of terahertz technology in neuroscience: current status and future perspective. *iScience* 24 (12), 1–11. doi:10.1016/j.isci.2021.103548

Zhang, M., Cheng, Q., Wang, B., Yang, L., Wang, J., Wu, R., et al. (2022b). Highly sensitive terahertz sensors based on polarization independent and multiple resonance. *Opt. Commun.* 507 (4), 127519–127531. doi:10.1016/j.optcom.2021.127519

Zhang, X., Wang, Y., Yuan, X., Shen, Y., Lu, Z., and Wang, Z. (2022a). Adaptive dynamic surface control with disturbance observers for battery/supercapacitor-based hybrid energy sources in electric vehicles. *IEEE Trans. Transp. Electrification*, 1. doi:10.1109/TTE.2022.3194034

Zhang, Z., Xiao, Y., Ma, Z., Xiao, M., Ding, Z., Lei, X., et al. (2019). 6G wireless networks: vision, requirements, architecture, and key technologies. *IEEE Veh. Technol. Mag.* 14 (3), 28–41. doi:10.1109/mvt.2019.2921208

Zhao, F., Zhu, C., Guo, W., Cong, J., Tee, C., Song, C., et al. (2019a). Resonant tunneling diode (RTD) terahertz active transmission line oscillator with graphene-plasma wave and two graphene antennas. *Electronics* 8 (10), 1164–1216. doi:10.3390/electronics8101164

Zhao, L., and Wang, L. (2022). A new lightweight network based on MobileNetV3. *KSII Trans. Internet Inf. Syst.* 8 (3), 1–15. doi:10.3837/tiis.2022.01.001

Zhao, S., Hu, F., Xu, X., et al. (2019b). Electrically triggered dual-band tunable terahertz metamaterial band-pass filter based on Si_3N_4-VO_2-Si_3N_4 sandwitch. *Chin. Phys. B* 28 (5), 115–120. doi:10.1088/1674-1056/28/5/054203

Zhao, Z., Xu, G., Zhang, N., and Zhang, Q. (2022). Performance analysis of the hybrid satellite-terrestrial relay network with opportunistic scheduling over generalized fading channels. *IEEE Trans. Veh. Technol.* 71 (3), 2914–2924. doi:10.1109/TVT.2021.3139885

Zhou, D., Sheng, M., Li, J., and Han, Z. (2023). Aerospace integrated networks innovation for empowering 6G: A survey and future challenges. *IEEE Commun. Surv. Tutorials* 25 (2), 975–1019. doi:10.1109/COMST.2023.3245614

Zhu, S. Y., Li, Y. L., Luk, K. M., and Pang, S. W. (2020). Compact high-gain si-imprinted THz antenna for ultrahigh speed wireless communications. *IEEE Trans. Antennas Propag.* 68 (8), 5945–5954. doi:10.1109/tap.2020.2986863

Zou, H., and Chen, Y. (2020). A thermally tunable terahertz three-dimensional perfect metamaterial absorber for temperature sensing application. *Mod. Phys. Lett. B* 34 (18), 207–219. doi:10.1142/S0217984920502073